Materials Chemistry and Physics 332 (2025) 130237

Contents lists available at ScienceDirect

Materials Chemistry and Physics

journal homepage: www.elsevier.com/locate/matchemphys

Exploring Fe^{3+} cation exchange dynamics in fluorescent MIL-53(Al) MOF: Solid-state photoluminescence and structural insights

T. Ul Rehman *, S. Agnello, F.M. Gelardi, M.M. Calvino, G. Lazzara, G. Buscarino, M. Cannas

Dipartimento di Fisica e Chimica—Emilio Segrè, Università degli Studi di Palermo, 90123, Palermo, Italy

HIGHLIGHTS

- Investigation of Fe^{3+} cation exchange in MIL-53(Al) MOF using diverse structural and optical techniques.
- Effects of different activation temperatures on solid-state photoluminescence (PL).
- Enhanced thermal stability upon Fe^{3+} incorporation.
- UV and visible photoluminescence (PL) quenching correlated with Fe^{3+} concentration.
- Interplay between cation exchange, structural modifications, and luminescence.

GRAPHICAL ABSTRACT

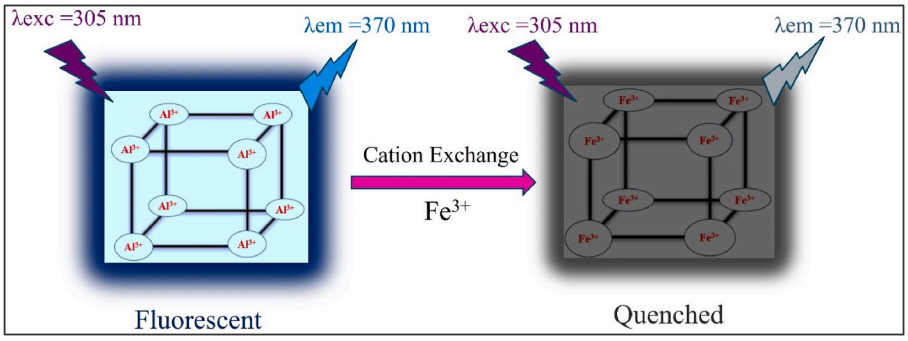

ARTICLE INFO

Keywords:
Metal-organic frameworks
MIL-53(Al)
Fe^{3+} ion exchange
Time-resolved Photoluminescence spectroscopy
Fourier-transform Raman spectroscopy
Powder X-ray diffraction
Thermogravimetric analysis

ABSTRACT

Flexible luminescent MOFs have gained significant interest since they combine the advantages of ratiometric fluorescence with the ability to modify the structure to accommodate a large variety of guest molecules. This study has investigated the influence of different concentrations of Fe^{3+} cations on the MIL-53(Al) MOF by employing a comprehensive array of characterization techniques on the solid-state samples, aiming to relate the optical response with the structural modifications. Structural and thermogravimetric findings evidenced modifications in peak positions, intensities, and an improved thermal stability of Fe^{3+}-exchanged MIL-53(Al) samples compared to the pristine MOF, thus indicating structural changes induced by the incorporation of Fe^{3+} cations. Moreover, as the Fe^{3+} concentration increases, a quenching of the UV and blue photoluminescence bands is observed. Hence, shedding light on the complex interplay between Fe^{3+} cation exchange, the photoluminescence and structural properties of solid-state MIL-53(Al) MOF, can provide valuable insights for the rational design and engineering of MOF-based materials for various applications, including sensing, catalysis, and optoelectronics.

1. Introduction

Metal ions play essential roles in numerous biological, environmental, and industrial processes, making their detection and quantification crucial for various applications, ranging from environmental monitoring to biomedical diagnostics [1–3]. Among these metal ions, Fe^{3+} holds significant importance due to its ubiquitous presence and diverse functions in biological systems [1,4,5]; they are indeed vital

* Corresponding author.
E-mail address: tanzeelul.rehman@unipa.it (T.U. Rehman).

https://doi.org/10.1016/j.matchemphys.2024.130237
Received 19 August 2024; Received in revised form 18 November 2024; Accepted 1 December 2024
Available online 7 December 2024

for human health, acting as cofactors in enzymatic reactions involved in oxygen transport, DNA synthesis, and cellular respiration [4–7]. However, excessive levels of Fe^{3+} ions can result in oxidative stress, DNA damage, and various pathological conditions, including neurodegenerative diseases like Alzheimer's and Parkinson's [8–10]. Fe^{3+} contamination in environmental matrices can result as well from human activities such as mining, industrial discharge, and agricultural runoff, posing environmental hazards and health risks to ecosystems and human populations [11–14]. Therefore, precise monitoring and regulation of Fe^{3+} ion concentrations are critical for maintaining physiological balance and preventing adverse health effects [1,4,5,7,8,10].

To address the pressing need for sensitive and selective detection of Fe^{3+} ions, extensive efforts have been devoted to developing advanced sensing platforms with high sensitivity, selectivity, and tunable performance [1,3,5]. Recent studies have highlighted the potential of Metal-Organic Frameworks (MOFs), particularly photoluminescent (PL)-active MOFs, as effective materials for metal ion sensing due to their high surface area, tunable porosity, and functional adaptability [15–17]. MOFs with photoluminescence properties offer rapid, visual detection of Fe^{3+} ions, with mechanisms influenced by structural composition, surface morphology, and charge transfer processes, such as ligand-to-metal (LMCT) and metal-to-ligand (MLCT) transitions [17]. While materials like quantum dots (QDs) and functionalized graphene oxide nanostructures have also shown potential for Fe^{3+} detection but challenges such as short-wavelength emission, limited Stokes shift, low quantum yield, and insufficient selectivity have constrained their effectiveness for Fe^{3+} detection [18,19].

Among luminescent MOFs, MIL-53(Al) stands out as an exceptional platform for selective Fe^{3+} ion sensing due to its inherent flexibility, chemical stability, and high affinity for specific metal ions [20–22]. In comparison to other MOFs, such as those based on Cu and Zn metal clusters, which have demonstrated good sensitivity but often lack chemical and thermal stability, MIL-53(Al) exhibits superior performance in both sensitivity and stability under environmental conditions [20–24]. Recent studies indicate that MIL-53(Al) demonstrates substantial sensitivity for Fe^{3+} detection without necessitating complex functionalization, as required by other flexible luminescence MOFs, such as luminescent UiO-66, which frequently require modification with specific ligands to enhance metal ion selectivity and stability [20,25]. Furthermore, the distinctive photoluminescent properties of MIL-53(Al) enable a weak luminescence signal upon Fe^{3+} binding, facilitated by mechanisms such as charge transfer quenching and energy transfer effects, even in the presence of competing ions [17,20,21].

Beyond Fe^{3+} sensing, over the past decade MOFs have also been employed for the generation of electrochemical and photochemical energy, particularly for oxygen evolution reaction (OER), and for the storage of chemical hydrogen as a gaseous fuel via the catalytic activity. The catalytic activity of MOFs stems from their organic linkers and metal nodes, which serve as active sites, further addressing their versatility and applicability across multiple scientific and industrial domains [26–28].

In this work we investigate the solid-state MIL-53(Al) MOF and its potential for sensing Fe^{3+} ions through controlled cation exchange processes. By performing Fe^{3+} cation exchange experiments, we aim to unveil the structural properties, thermal stability, and the solid-state PL properties. We opted to perform a comprehensive investigation involving optical spectroscopy, thermal and structural characterizations, to understand the impact of Fe^{3+} cation exchange on MIL-53(Al) MOF, activated at different temperatures. Our findings not only contribute to the fundamental understanding of MOF behaviour but also hold immense potential for the development of advanced sensing platforms with tailored selectivity and sensitivity towards Fe^{3+} ions. By utilizing the unique properties of MIL-53(Al) MOF, we aim to pave the way towards the realization of next-generation sensing technologies capable of addressing the ever-growing demands for efficient metal ion detection and monitoring in diverse real-world scenarios.

2. Materials and methods

MIL-53(Al) and its organic ligand, terephthalic acid (BDC, 99 %+) are provided by Sigma-Aldrich (Sigma-Aldrich S.r.l., Milan, Italy). We investigated two series of samples: the first was prepared by activating the raw powder in a glass tube at 120 °C for 12 h and then sealing it, and is referred to as MIL-53(Al), activated (120 °C); the second was prepared by activating the MIL-53(Al) powder in a glass tube at 300 °C for 24 h, and is referred to as MIL-53(Al), activated (300 °C). Additionally, 25 mg of MIL-53(Al) powder were dispersed in 5 mL of Fe^{3+} solution at different concentrations (0.1−100 mM) for the cation exchange experiment. After that, the suspension was centrifuged for 5 min at 10,000 rpm to extract the MIL 53(Al) powder. Following three rounds of washing with ultrapure water, the MIL-53(Al) powder was heated at 120 and 300 °C for a duration of 12 and 24 h, respectively.

The crystalline structure of MIL-53(Al) was analysed through Powder X-ray diffraction (PXRD) method, using a Rigaku Miniflex diffractometer with a Cu Kα source (1.541 Å). Diffraction data was collected at a 0.01° step size, 1°/min, with a range of 2θ angles from 7° to 70°. To evaluate the thermal stability of MIL-53(Al), thermogravimetric analysis (TGA) and differential thermal analysis (DTA) were performed. The experiments were conducted on a TGA 550 (Discovery Series – TA Instruments) with each sample heated in a platinum pan from room temperature to 800 °C at a scanning rate of 20 °C/min, respectively.

The influence of Fe^{3+} ions on the vibrational spectra of MIL-53(Al) was examined using FT-Raman spectroscopy. The experiments were performed on a Bruker Vertex 70v RAMII spectrometer using a Nd:YAG laser with a wavelength of 1064 nm and a power of 500 mW as the excitation source. The spectra reported in this work were recorded with a spectral resolution of 2.5 cm^{-1}, averaging over 200 scans.

Time resolved photoluminescence spectroscopy (TRPL) was used to investigate the emission bands of solid-state MIL-53(Al) samples and the kinetics decay. The excitation source consisted of an optical parametric oscillator (VIBRANT OPOTEK) pumped by the third harmonic (3.49 eV) of a Nd:YAG laser with a pulse width of 5 ns and a repetition rate of 10 Hz. The emitted light was analysed using a monochromator equipped with a grating of 150 lines/mm and a blaze wavelength of 300 nm and acquired using an intensified CCD camera that was driven by a delay generator (PIMAX Princeton Instruments). We set the acquisition time window (TW) and delay (TD) with respect to the laser pulses and detected the emission spectra with a bandwidth of 5 nm while correcting for the monochromator dispersion.

3. Results and discussion

3.1. Powder x-ray diffraction

Structural analysis of MIL-53(Al) samples activated at 120 °C and 300 °C was conducted using PXRD method and presented in Fig. 1. To broaden the scope of our analysis, we also compared these findings with pertinent data from scientific literature, which are depicted as vertical dashed lines, with the thickness of the lines representing the intensity of the corresponding peaks [29]. The PXRD results revealed that in both cases, the crystal structure of MIL-53(Al) had a mixed pore structure, as evidenced by the peaks originating at the d-spacing of 10.50 Å, 6.0 Å, and 5.12 Å, which are characteristic of large pore (LP) structure and represented by the blue vertical dotted lines in Fig. 1. In addition, the peaks originating at the d-spacing of 9.70 Å, 7.30 Å, and 4.82 Å are indicative of hydrated narrow pore (NP-h) structure and are represented by the green vertical dotted lines in Fig. 1 [29,30]. Furthermore, there is a minor shift in d-spacing and an increase in the relative intensities of the peaks in the case of MIL-53(Al) activated at 300 °C compared to the one activated at 120 °C, respectively.

Additionally, the cation exchange of metal node Al^{3+} in MIL-53(Al) with Fe^{3+} was also monitored using PXRD patterns. As shown in Fig. 2 (A), cation exchange of Al^{3+} metal nodes in MOF with Fe^{3+} also causes

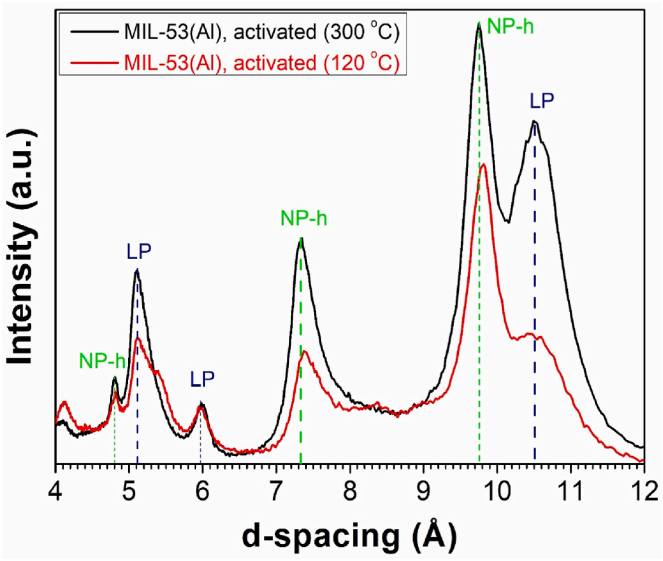

Fig. 1. PXRD of MIL-53(Al) samples activated at 120 °C and 300 °C.

the amorphization of the framework, resulting in the conversion of MIL-53(Al) to MIL-53(Fe). As the concentration of Fe^{3+} increased, the PXRD patterns for MIL-53(Al) gradually changed to that of MIL-53(Fe), and the intensity of the corresponding Bragg's peaks decreased considerably [31]. In Fig. 2(B), The normalised zoomed-in diffraction patterns also showed a shift of the main Bragg's peaks towards the lower d-spacing with the higher concentration of Fe^{3+} ions.

3.2. Thermogravimetric analysis

Fig. 3(A) and (B) depicts the TGA and DTA of the MIL-53(Al) MOF activated at 120 °C and 300 °C. The sample activated at 300 °C shows two weight losses, one below 100 °C and the second above 500 °C, while the sample activated at 120 °C exhibits an additional weight loss from 330 °C to 430 °C, respectively. According to these results, the initial weight loss in both samples is attributed to the removal of moisturizers from the MOF surface, followed by the desorption of strongly bonded water molecules inside the cavities and the decomposition of organic linkers from the sample activated at 120 °C. Additionally, the third weight loss is attributed to the decomposition of the framework. These findings are consistent with the PXRD spectra of both samples, as the diffraction peaks are more intense and sharper in the case of the sample activated at 300 °C compared to the one activated at 120 °C, respectively.

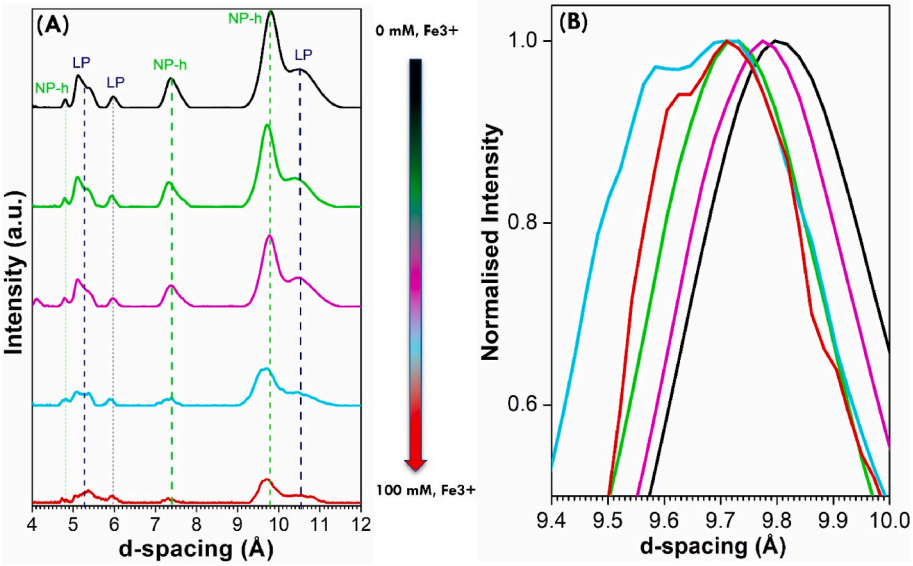

Fig. 2. (A) Powder x-ray diffraction (PXRD) patterns of MIL-53(Al) with the concentration of $Fe3^{+}$ from 0 to 100 mM. (B) Normalised zoomed in XRD patterns from 9.4 to 10 Å.

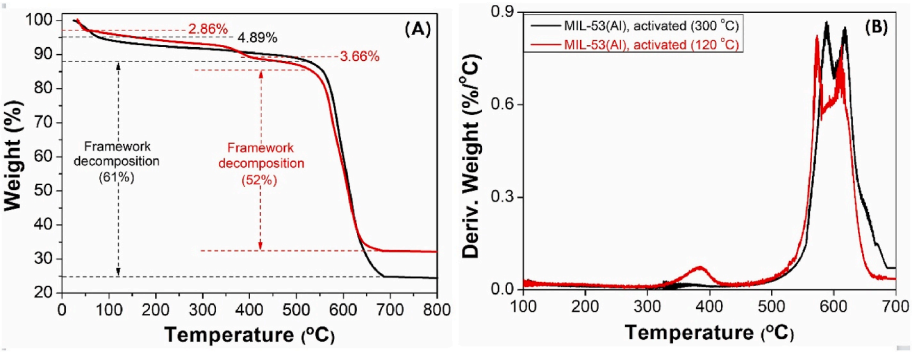

Fig. 3. (A) Thermogravimetric analysis (TGA) and (B) differential thermal analysis (DTA) of MIL-53(Al) activated at 120 °C (red lines) and 300 °C (black lines). (For interpretation of the references to colour in this figure legend, the reader is referred to the Web version of this article.)

As shown in Fig. 4(A) and (B), TGA and DTA were also conducted to examine the thermal stability and decomposition behaviour of MIL-53 (Al) exposed to Fe^{3+} ion exchange at varying concentrations (0–100 mM). Notably, three distinct weight loss curves were observed for all samples, indicating the occurrence of multiple decomposition processes within the temperature range of analysis. For samples containing Fe^{3+} ion concentrations ranging from 0 mM to 5 mM, the TGA curves showed weight loss events at temperatures of 100 °C, 300 °C, and 500 °C, respectively: the initial step can be attributed to the loss of physically and chemically bound water or solvent molecules within the MOF; the second likely corresponds to the strongly bound water molecules within the cavities of the framework and the decomposition of organic ligands or linker molecules; the third may indicate the decomposition of residual organic moieties or the collapse of the MOF framework [32,33]. In contrast, as shown in Fig. 4(B), for samples with Fe^{3+} ion concentrations ranging from 50 mM to 100 mM, a significant shift in the temperature range of the first weight loss event was observed, occurring between 120 °C and 200 °C. Furthermore, the magnitude of the weight loss observed above 500 °C in these samples was significantly lower compared to those with lower Fe^{3+} ion concentrations or the pristine MIL-53(Al) MOF. These findings highlight the importance of Fe^{3+} ion exchange dynamics in modulating the thermal properties of the MOF. The observed shifts in weight loss temperatures and changes in decomposition profiles contribute to the understanding of MOF behaviour and have implications for applications requiring precise control over thermal stability and decomposition characteristics.

3.3. Fourier-transform Raman spectroscopy

The cation exchange of metal node Al^{3+} in MIL-53(Al) with Fe^{3+} was also monitored using FT-Raman spectroscopy. As depicted in Fig. 5, there are six vibrational bands in the frequency range of 850 cm^{-1} to 3100 cm^{-1}. The vibrational mode in the frequency range of 860–885 cm^{-1} is attributed to the bending of aromatic rings and bending of carboxyl groups from the organic linker ($\delta CCC + \delta CO_2$). For better understanding, the zoomed-in spectra of all the vibrational modes are also presented in Fig. 6. It appears in Fig. 6 (A) that with the highest content of Fe^{3+} ions, the vibrational bands centred at 872 cm^{-1} and 878 cm^{-1} shift to 874 cm^{-1} and 880 cm^{-1}, respectively. Additionally, as shown in Fig. 5, vibrational modes in the frequency range from 1135 to 1160 cm^{-1} appear and are associated with the stretching of carboxyl groups and aromatic ring + H atoms rocking on the aromatic ring ($\nu CC + \delta CH$) [29]. As shown in Fig. 6 (B), it is observed that the centre of this first vibration band is shifted from 1144 cm^{-1} to 1145 while the second vibrational mode is shifted from 1149 cm^{-1} to 1153 cm^{-1} with the highest Fe^{3+} content.

Additionally, as shown in Fig. 5, the vibrational bands in the frequency range from 1592 to 1634 cm^{-1} are attributed to the asymmetric stretching vibration ($\nu asCO(CO_2)$) modes of the carboxylate groups of the organic linkers, with corresponding symmetric stretching vibration

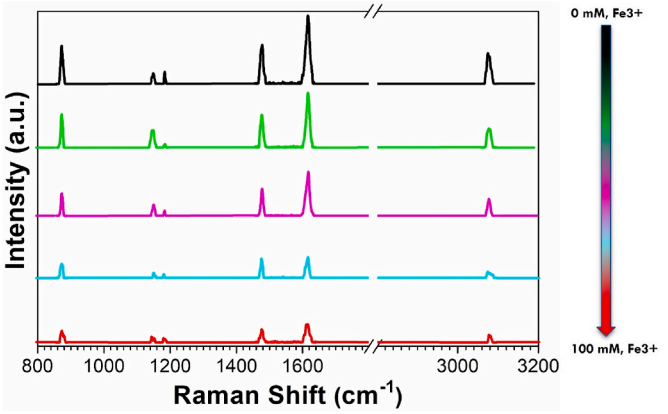

Fig. 5. Fourier-transform Raman (FT-Raman) spectroscopy of MIL-53(Al) with the concentration of Fe^{3+} ions 0–100 mM.

($\nu sCO(CO_2)$) modes appearing in the frequency range of 1463–1490 cm^{-1}. As depicted in Fig. 6 (C), the band centred at 1476 cm^{-1}, as well as the band centred at 1617 cm^{-1} become structured on increasing the Fe^{3+} content. Moreover, as displayed in Fig. 6 (D), vibrational modes in the frequency range from 3060 to 3085 cm^{-1} are also found and can be attributed to the stretching vibration of aromatic (νCH) C–H bonds [29]. It is also important to notice that the Fe^{3+} cation exchange significantly reduces the relative intensity of all Raman peaks and modifies the shapes of the vibrational spectra as well, the centre of the –CH stretching vibration band is indeed shifted from 3076 cm^{-1} to 3079 cm^{-1}.

3.4. Time-resolved photoluminescence spectroscopy

TRPL spectroscopy was employed to analyse the emission properties of pristine solid-state MIL-53(Al) MOF samples activated at two different temperatures, as well as the free BDC organic linkers, respectively; all the samples were excited at 305 nm. As shown in Fig. 7(A), the PL spectra of MIL-53(Al) activated at 120 °C presents a single emission peak centred around 370 nm, indicating the presence of a specific chromophore within the MOF framework. In contrast, MIL-53(Al) activated at 300 °C exhibits two distinct emission bands, with peaks centred around 380 nm and 442 nm, respectively. This suggests the existence of multiple luminescent species or electronic transitions within the MOF structure induced by the activation process. The emission spectrum of the free BDC organic linkers showed a single peak centred at 390 nm, suggesting differences in the luminescent behaviour of the linker when incorporated into the MOF framework compared to the pristine form.

Moreover, PL decay measurements revealed variations in the lifetimes of excited states amongst all the samples. As shown in Fig. 7(B), all curves, monitored at 380 nm, were well fitted by a single exponential decay function: MIL-53(Al) activated at 300 °C and 120 °C exhibited a

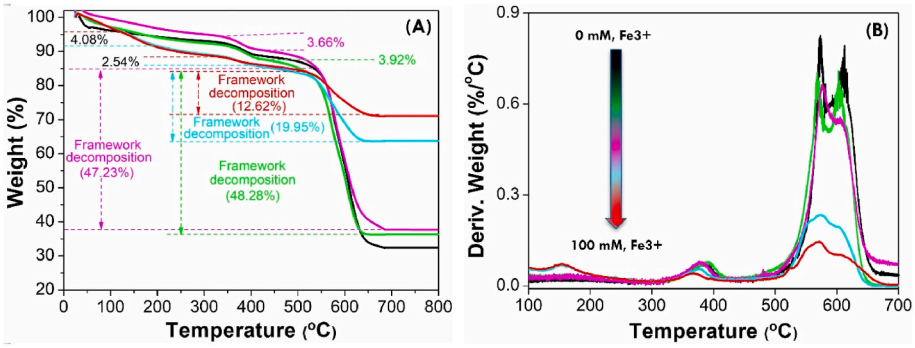

Fig. 4. (A) Thermogravimetric analysis (TGA) and (B) differential thermal analysis (DTA) of MIL-53(Al) with the concentration of Fe^{3+} ions 0–100 mM.

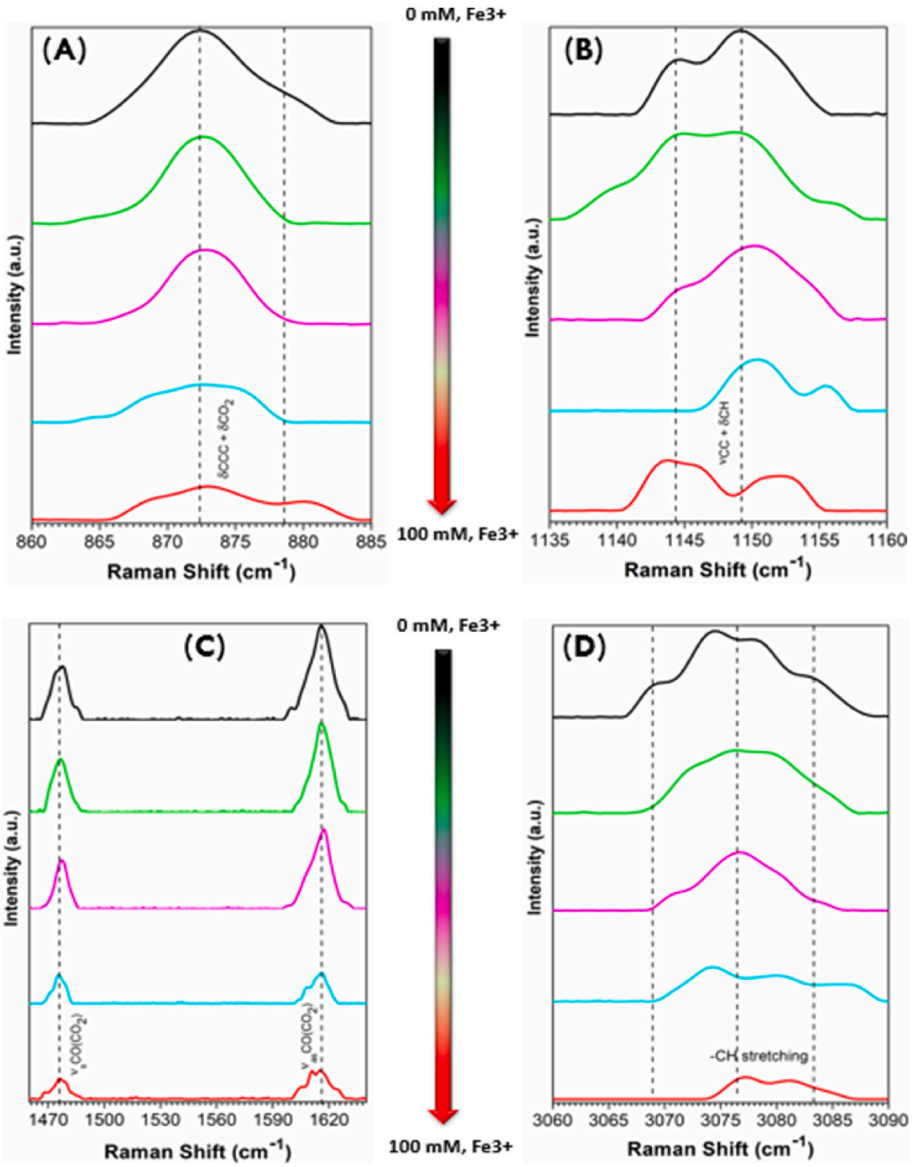

Fig. 6. (A) (B) (C) and (D) are the zoomed-in FT-Raman spectra of MIL-53(Al) in different spectral ranges with the concentration of Fe^{3+} ions from 0 to 100 mM.

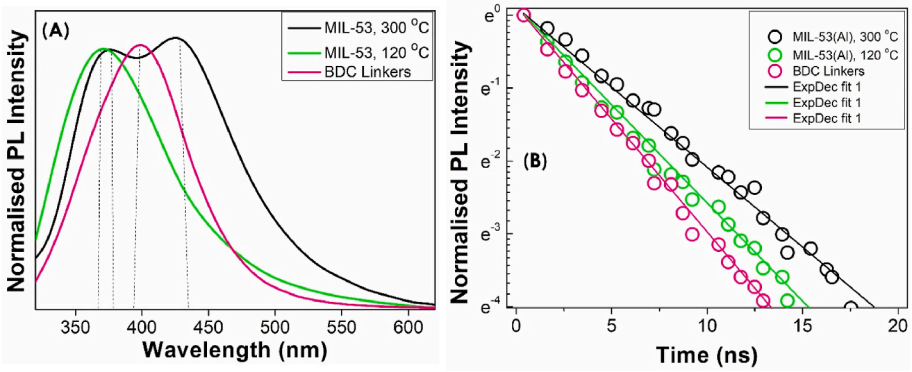

Fig. 7. (A) Normalised emission spectra of MIL-53(Al) activated at 120 °C (for 12 h) and 300 °C (for 24 h), in comparison with free BDC linkers when excited at 305 nm. (B) photoluminescence time decay curves monitored at 380 nm, (circles) and best-fitted curves (solid lines).

lifetime $\tau = 6.5 \pm 0.3$ ns and $\tau = 4.7 \pm 0.3$ ns, respectively; free BDC linkers exhibited a lifetime $\tau = 3.8 \pm 0.2$ ns. These results clearly indicate that the presence of different activation processes in the MOF structure significantly affect the luminescent behaviour and the lifetimes of the excited states [34].

TRPL spectroscopy was also carried out on the solid-state MIL-53(Al)

MOF samples that underwent cation exchange with Fe^{3+} ions at concentrations ranging from 0 to 100 mM. These samples were also activated at 120 °C and 300 °C to evaluate the impact of activation temperature on PL behaviour. As shown in Fig. 8(A), the emission spectra of MIL-53(Al) samples activated at 120 °C exhibited a single emission peak centred around 370 nm, like the pristine sample; however, the PL intensity decreased as the Fe^{3+} ion concentration increased. Correspondingly, as shown in Fig. 8(B), MIL-53(Al) samples activated at 300 °C exhibited two distinct emission bands, with peaks centred around 380 nm and 442 nm, respectively, the intensity of both bands decreased with higher Fe^{3+} ion concentrations. Previous research has shown that the luminescence quenching of MOFs by metal cations occurs through three primary mechanisms: (1) interactions between metal cations and organic ligands, (2) structural collapse induced by metal cations, and (3) cation exchange, where central framework cations are replaced by targeted cations. Particularly, relevant to this study is the transition of MIL-53(Al) to MIL-53(Fe) via cation exchange between Fe^{3+} and the framework's Al^{3+}. Based on these findings, we hypothesize that the significant quenching effect of MIL-53(Al) by Fe^{3+} results cation exchange [35].

The PL lifetimes were also measured to investigate the dynamics of luminescent species in solid-state MIL-53(Al) MOF samples that had been cation-exchanged with Fe^{3+} ions at concentrations ranging from 0 mM to 100 mM. As presented in Fig. 9(A), the lifetimes curves were measured in MIL-53(Al) samples activated at 120 °C for 12 h at the emission maximum of 370 nm. The lifetimes were measured as $\tau = 5.0 \pm 0.3$ ns, $\tau = 4.0 \pm 0.2$ ns, $\tau = 3.0 \pm 0.2$ ns, $\tau = 2.0 \pm 0.1$ ns, and $\tau = 1.7 \pm 0.1$ ns for Fe^{3+} ion concentrations ranging from 0 mM to 100 mM, respectively. Similarly, as presented in Fig. 9(B), decay curves were recorded at 380 nm in MIL-53(Al) samples activated at 300 °C for 24 h and the lifetimes were measured as $\tau = 6.5 \pm 0.3$ ns, $\tau = 4.6 \pm 0.3$ ns, $\tau = 3.7 \pm 0.2$ ns, $\tau = 2.8 \pm 0.2$ ns, and $\tau = 2.1 \pm 0.1$ ns. Furthermore, as presented in Fig. 9(C), decay curves recorded at 442 nm exhibited the lifetimes $\tau = 10.0 \pm 0.4$ ns, $\tau = 6.2 \pm 0.3$ ns, $\tau = 3.8 \pm 0.2$ ns, $\tau = 2.8 \pm 0.2$ ns, and $\tau = 2.2 \pm 0.1$ ns for Fe^{3+} ion concentrations ranging from 0 mM to 100 mM, respectively. Overall, these results demonstrate the influence of Fe^{3+} ion concentration and activation temperature on the dynamics of the luminescent of MIL-53(Al) MOF. The observed decrease in PL lifetimes suggests the presence of quenching mechanisms induced by Fe^{3+} ions, which affect the competition between radiative and non-radiative recombination processes from the excited states within the MOF framework [35–37].

4. Discussion

In PXRD patterns the observed structural changes of MIL-53(Al) MOF samples, with higher concentrations of Fe^{3+} ions, is attributed to several factors, including changes in the coordination environment, differences in ionic size, and ion exchange dynamics. Fe^{3+} ions may introduce structural distortions or alter the coordination environment of metal clusters and organic linkers within the MOF framework, destabilizing the crystal lattice and promoting disorder. Additionally, the larger size of Fe^{3+} ions may lead to steric hindrance and strain within the MOF structure, further promoting disorder and amorphization. The process of cation exchange involves the replacement of original cations Al^{3+} with Fe^{3+} ions, and the kinetics and extent of this exchange process can vary depending on factors such as Fe^{3+} ion concentration, reaction conditions, and the nature of the MOF structure. Higher concentrations of Fe^{3+} ions may lead to more extensive ion exchange and amorphization of the crystalline framework. Overall, the observed changes in the PXRD patterns of MIL-53(Al) samples with higher concentrations of Fe^{3+} ions are a consequence of structural perturbations induced by Fe^{3+} ion incorporation. These perturbations can lead to disorder, loss of crystallinity, and a decrease in PXRD peak intensities, highlighting the sensitivity of MOF structures to changes in composition and coordination environment [35,38].

The reduction in weight loss observed during the thermal decomposition of MIL-53(Al) MOF upon Fe^{3+} cation exchange can be ascribed to several factors. Firstly, the incorporation of Fe^{3+} ions into the MIL-53 (Al) framework leads to the formation of stronger metal-ligand bonds or coordination interactions, which can stabilize the MOF structure and make it more resistant to thermal decomposition. As a result, the extent of weight loss associated with framework decomposition decreases with increasing Fe^{3+} ion concentration. Secondly, Fe^{3+} ions have higher coordination numbers and stronger metal-ligand interactions than Al^{3+} ions, which can enhance the thermal stability of the MOF framework, delaying or inhibiting the onset of decomposition processes at elevated temperatures. Thirdly, the presence of Fe^{3+} ions within the MOF structure may alter the pathways and kinetics of thermal decomposition processes, leading to changes in the overall decomposition behaviour of the MOF. Lastly, the extent of weight loss reduction may correlate with the concentration of Fe^{3+} ions exchanged into the MIL-53(Al) framework, with higher concentrations leading to more significant stabilization effects. Additionally, the observed decrease in weight loss during TGA analysis of Fe^{3+} cation-exchanged MIL-53(Al) samples is indicative of enhanced thermal stability and structural integrity conferred by Fe^{3+} ion incorporation. These findings highlight the potential of cation exchange strategies for modulating the thermal properties and stability of MOF materials, with implications for various applications including gas storage, catalysis, and thermal insulation.

The decrease in intensity, disruption in shape, and frequency shift of Raman peaks observed in MIL-53(Al) samples upon Fe^{3+} cation exchange can be attributed to various factors. These include ionic size differences, disorder induced by cation exchange, electronic effects, and redistribution of vibrational energy. Fe^{3+} ions have a larger ionic radius than Al^{3+} ions, which can introduce strain and distortions in the lattice structure, leading to broadening and weakening of Raman peaks. Furthermore, electronic interactions between Fe^{3+} ions and organic

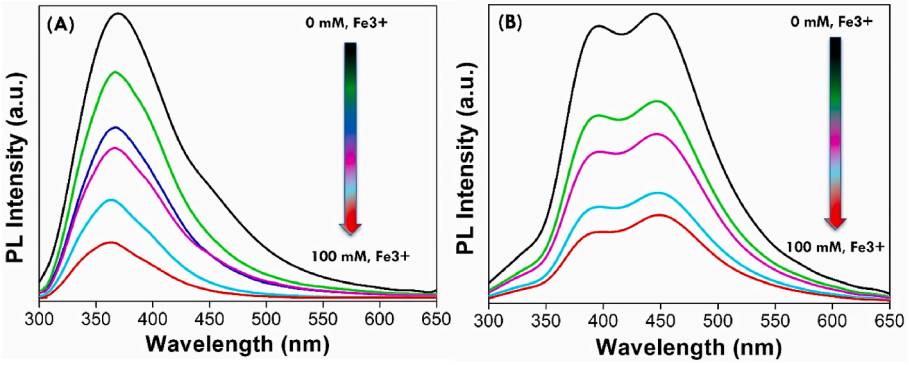

Fig. 8. (A) Photoluminescence (PL) emission spectra of MIL-53(Al) with the concentration of Fe^{3+} from 0 to 100 mM when activated at 120 °C for 12 h. (B) Photoluminescence (PL) spectra of MIL-53(Al) with the concentration of Fe^{3+} from 0 to 100 mM when activated at 300 °C for 24 h.

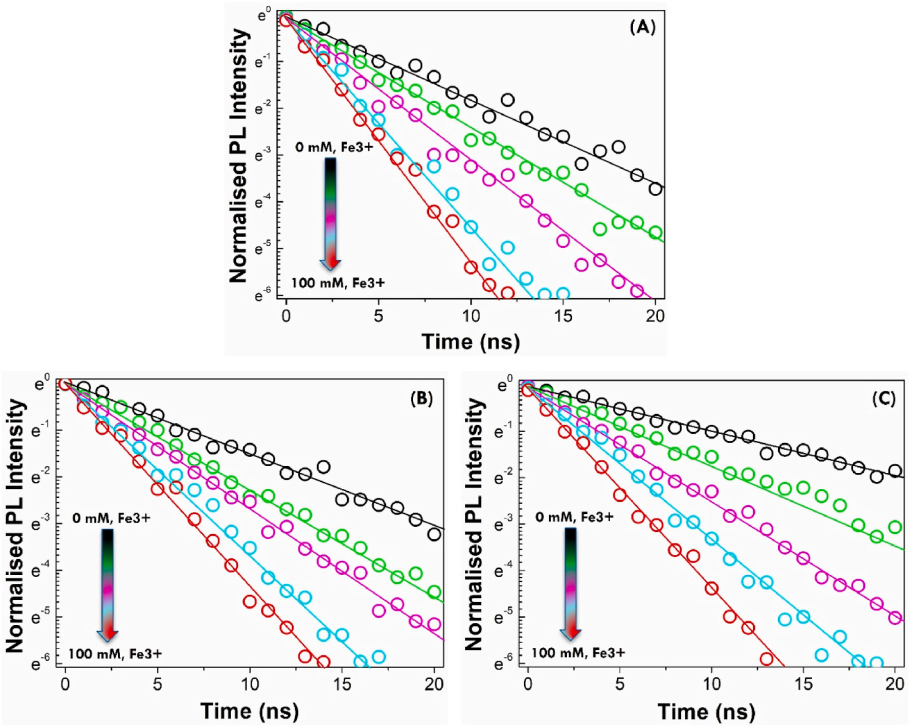

Fig. 9. (A) Lifetimes curves of MIL-53(Al), taken from the emission maxima of 370 nm, with the concentration of Fe^{3+} from 0 to 100 mM when activated at 120 °C for 12 h. (B) and (C) Lifetimes curves of MIL-53(Al), taken from the emission maxima of 380 and 442 nm, with the concentration of Fe^{3+} from 0 to 100 mM when activated at 300 °C for 24 h.

ligands within the MOF framework can influence the vibrational properties of the material and contribute to spectral changes in FT-Raman measurements. Finally, the presence of Fe^{3+} ions can affect the distribution of vibrational modes within the MIL-53(Al) framework, resulting in changes in the intensity, shape, and frequency of Raman peaks, reflecting alterations in the vibrational dynamics of the material induced by Fe^{3+} ion incorporation.

In Fig. 10(A), the emission spectra of molecular organic linkers (free BDC) and solid-state MIL-53(Al) samples activated at 300 °C and 120 °C are presented. It is evidenced that the organic linkers in the free BDC (terephthalic acid) molecular form have fluorescence emission maximum at 390 nm, the origin of this PL is likely owing to the transitions between the lowest excited singlet state and the singlet ground state, involving π-π* or n-π* transitions [17]. As depicted in Fig. 10(A), the lower PL intensity and the shorter lifetime, as well as the observed shift in the photoluminescence (PL) emission band compared to the MOF samples, could be attributed to the absence of structural rigidity provided by the MOF framework, leading to increased non-radiative decay rates [34,36].

The MIL-53(Al) MOF sample activated at 120 °C displayed a single emission band at 370 nm, that arises from transitions within the organic linkers (intra-ligand transitions), similar to the free BDC organic linkers (π-π* or n-π*) [34]. However, the presence of the MOF framework likely stabilizes the excited state of the ligand, reducing non-radiative decay rates and enhancing fluorescence intensity compared to the molecular BDC linkers. The structural rigidity provided by the MOF framework

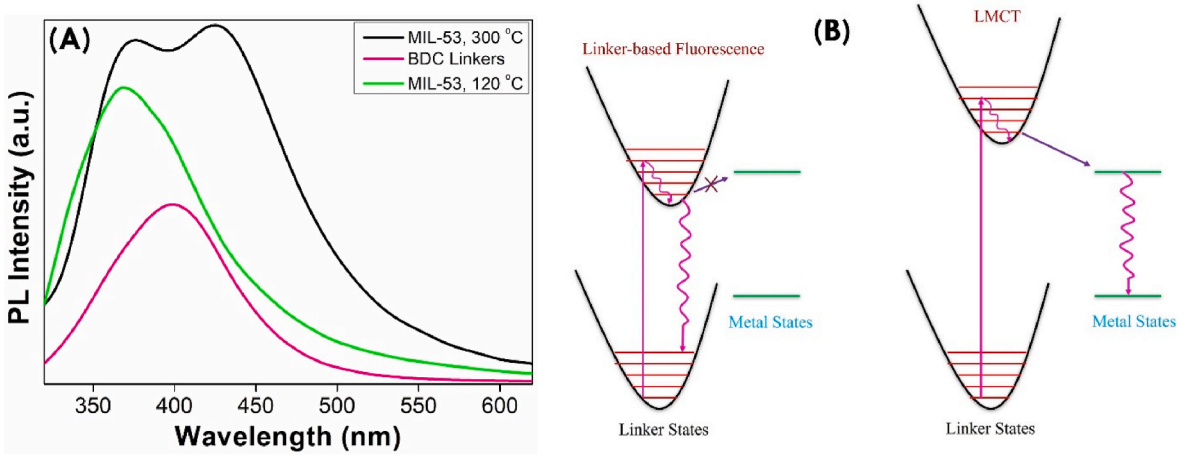

Fig. 10. (A) Photoluminescence (PL) emission spectra of MIL-53(Al) activated at 120 °C (for 12 h) and 300 °C (for 24 h), in comparison with free BDC linkers when excited at 305 nm. (B) Energy level diagram representing the organic linker's HOMO and LUMO energy states as well as the intersystem crossing (LMCT) that leads to emissive metal states.

may also contribute to the observed emission characteristics. Moreover, the MIL-53(Al) MOFs illustrate the effect of increasing linker conjugation. When this occurs, as shown on the left side of Fig. 10(B), the π-π* energy gap decreases, making energy transfer to the metal less efficient. If π-conjugation in the ligand is increased, the HOMO-LUMO gap is decreased, making ligand to metal charge transfer (LMCT) inefficient and, therefore, ligand-based emission is observed. Additionally, coupling to surrounding solvent or guest molecules may also affect the efficiency of these transitions for porous structures. The resulting ligand-based emission resembles that of the corresponding ligand in dilute solutions, respectively [39]. These arguments are further supported by the PXRD and TGA analysis, as the intensity of all the Bragg's peaks in this sample is less as compared to the one activated at 300 °C, as well as the confirmation of additional weight loss from 330 °C to 430 °C evidences the presence of strongly bonded water molecules within the MOF, playing a pivotal role in the photoluminescence (PL) properties of MIL-53(Al) MOF.

The most intriguing findings were observed in the MOF sample activated at 300 °C, which exhibited two emission bands centred at 380 nm and 442 nm in time-resolved photoluminescence (TRPL) spectroscopy. The emission at 380 nm corresponds to ligand-based emission, similar to the MOF sample activated at 120 °C. However, the appearance of a second emission band at 442 nm suggests additional luminescence mechanisms. According to the literature, this second band is attributed to LMCT mechanism that occurs when there are sufficient electronic interactions between the organic ligand and the metal ions within the MOF framework. In this case, the higher activation temperature likely induced structural changes within the MOF, leading to stronger interactions between the BDC linker and metal ions. This increased interaction facilitates charge transfer from the ligand to the metal ions, resulting in the observed LMCT-based emission at 442 nm. In other words, as depicted in Fig. 10(B), if π-conjugation in the ligand is decreased, the HOMO-LUMO gap is enlarged considerably, consequently, making LMCT) efficient and, therefore, give rise to the PL emission. In short, the origin of luminescence in each sample can be attributed to different mechanisms. The free BDC organic linker exhibits ligand-centred luminescence, while both MOF samples exhibit a combination of ligand-based emission and LMCT, respectively. The variations in emission characteristics between the MOF samples can be attributed to differences in activation temperature, structural changes, and interactions within the MOF framework, highlighting the complex interplay between structural factors and luminescence properties in MIL-53(Al) MOFs [34,39].

Additionally, the quenching in photoluminescent (PL) intensity and the declining fluorescent lifetimes upon Fe^{3+} cation exchange can be ascribed to the substitution of Al^{3+} metal centers with heavier Fe^{3+} ions and the strong binding of these ions to the organic linkers within the MIL-53(Al) framework. As observed in Figs. 8 and 9, for all bands the reduction in photoluminescent (PL) intensity and lifetime is correlated. We express the lifetime in samples not loaded with Fe^{3+} as $\tau_0 = 1/k_0$, where the decay rate k_0 from the excited state includes radiative k_r and nonradiative k_{nr} rates, while the initial value of the photoluminescent (PL) intensity is related to the quantum efficiency $\eta_0 = kr \times \tau_0$. It can therefore be hypothesized that the introduction of Fe^{3+} ions increases the non-radiative rate by Δk and consequently both, the lifetime $\tau = 1/(k_0 + \Delta k)$ and the quantum yield $\eta = kr \times \tau$ decrease considerably. Based on our results, we can estimate $\Delta k = 1/\tau - 1/\tau_0$. Limiting the comparison between the initial value τ_0 and that measured in samples with 100 mM Fe^{3+} concentration, we get: $\Delta k \approx 3.9 \times 10^9$ Hz for the photoluminescent (PL) at 370 nm in the MIL-53(Al) sample activated at 120 °C; $\Delta k \approx 3.2 \times 10^9$ Hz, similarly, for the photoluminescent (PL) at 380 nm in the sample activated at 300 °C; $\Delta k \approx 3.5 \times 10^9$ Hz for the photoluminescent (PL) at 442 nm, respectively.

The incorporation of Fe^{3+} ions lead to the structural distortions and perturbations, which disrupt the electronic structure and energy levels of the MOF. Factors such as differences in ionic size, cation exchange dynamics and electronic effects contribute to this phenomenon. Moreover, the high spin states of Fe^{3+} ions enable them to act as effective photoluminescence (PL) quenchers through non-radiative decay pathways, competing with luminescent processes [40]. Fe^{3+} cation exchange results in quenching of PL intensity and shorter fluorescent lifetimes owing to the conversion of strong-luminescent MIL-53(Al) to weak-luminescent MIL-53(Fe), leading to non-radiative decay pathways [31,35]. These results emphasize the significance of comprehending the interactions between dopant ions and luminescent centers in MOF materials for creating efficient luminescent devices and applications.

5. Conclusions

The results reported in the present work highlight how the structural, thermal and solid-state emission properties of MIL-53(Al) MOF samples are modified by the incorporation of Fe^{3+} ions, with concentration ranging from 0 to 100 mM. It is observed that the cation exchange of Al^{3+} metal centers with Fe^{3+} ions strengthens metal-ligand bonds and enhances the thermal stability of the MOF framework. Moreover, the higher concentration of Fe^{3+} ions induces a correlated quenching of the UV and visible PL bands and a reduction in their lifetime; this trend indicates that the high spin states of Fe^{3+} ions act as PL quenchers because they introduce a further non-radiative rate Δk from the excited state. These findings are generally relevant because they help us to clarify the origin of the luminescence bands of MOFs such as: intra-ligand transitions and ligand to metal charge transfer for the UV and visible PL, respectively. Overall, this research emphasizes on the importance of understanding the potential of cation exchange strategies for tailoring the properties of MOF materials to meet the specific requirements for various applications, such as catalysis, gas storage, and luminescent devices.

CRediT authorship contribution statement

T. Ul Rehman: Writing – original draft, Investigation, Formal analysis, Conceptualization. **S. Agnello:** Writing – review & editing, Methodology. **F.M. Gelardi:** Visualization, Validation. **M.M. Calvino:** Investigation, Data curation. **G. Lazzara:** Visualization, Conceptualization. **G. Buscarino:** Writing – review & editing, Methodology, Conceptualization. **M. Cannas:** Writing – review & editing, Supervision, Methodology, Conceptualization.

Declaration of competing interest

The authors declare that they have no known competing financial interests or personal relationships that could have appeared to influence the work reported in this paper.

Data availability

Data will be made available on request.

References

[1] X. Zheng, W. Cheng, C. Ji, J. Zhang, M. Yin, Detection of metal ions in biological systems: a review, Rev. Anal. Chem. 39 (1) (2020) 231–246.
[2] B. Liu, J. Zhuang, G. Wei, Recent advances in the design of colorimetric sensors for environmental monitoring, Environ. Sci.: Nano 7 (8) (2020) 2195–2213.
[3] E. Ekrami, M. Pouresmaieli, P. Shariati, M. Mahmoudifard, A review on designing biosensors for the detection of trace metals, Appl. Geochem. 127 (2021) 104902.
[4] D.M. Chen, N.N. Zhang, C.S. Liu, M. Du, Template-directed synthesis of a luminescent Tb-MOF material for highly selective Fe 3+ and Al 3+ ion detection and VOC vapor sensing, J. Mater. Chem. C 5 (9) (2017) 2311–2317.
[5] S. Bothra, J.N. Solanki, S.K. Sahoo, Functionalized silver nanoparticles as chemosensor for pH, Hg2+ and Fe3+ in aqueous medium, Sensor. Actuator. B Chem. 188 (2013) 937–943.
[6] X. Yang, X. Chen, X. Lu, C. Yan, Y. Xu, X. Hang, J. Qu, R. Liu, A highly selective and sensitive fluorescent chemosensor for detection of CN−, SO 3 2− and Fe 3+ based on aggregation-induced emission, J. Mater. Chem. C 4 (2) (2016) 383–390.

[7] M.G. Skalnaya, A.V. Skalny, Essential Trace Elements in Human Health: a Physician's View, vol. 224, Publishing House of Tomsk State University, Tomsk, 2018, pp. 1–222.
[8] Z. Zhao, Iron and oxidizing species in oxidative stress and Alzheimer's disease, Aging Medicine 2 (2) (2019) 82–87.
[9] K. Wojtunik-Kulesza, A. Oniszczuk, M. Waksmundzka-Hajnos, An attempt to elucidate the role of iron and zinc ions in development of Alzheimer's and Parkinson's diseases, Biomed. Pharmacother. 111 (2019) 1277–1289.
[10] A.A. Belaidi, A.I. Bush, Iron neurochemistry in Alzheimer's disease and Parkinson's disease: targets for therapeutics, J. Neurochem. 139 (2016) 179–197.
[11] S. Han, S.U. Hassan, Y. Zhu, S. Zhang, H. Liu, S. Zhang, J. Li, Z. Wang, C. Zhao, Significance of activated carbon fiber as cathode in electro/Fe3+/peroxydisulfate oxidation process for removing carbamazepine in aqueous environment, Ind. Eng. Chem. Res. 58 (42) (2019) 19709–19718.
[12] R. Naveen, M.C. Rao, K. Syed, J. Shim, R. Koutavarapu, Exploring the mechanistic insights of Fe3+-doped LiZnBO3 nanosheets for visible light-driven photocatalytic degradation of mineral pollutants in wastewater, J. Environ. Chem. Eng. 11 (5) (2023) 110565.
[13] A. Rashid, M. Ayub, Z. Ullah, A. Ali, S.A. Khattak, L. Ali, X. Gao, C. Li, S. Khan, H. A. El-Serehy, P. Kaushik, Geochemical modeling source provenance, public health exposure, and evaluating potentially harmful elements in groundwater: Statistical and human health risk assessment (HHRA), Int. J. Environ. Res. Publ. Health 19 (11) (2022) 6472.
[14] N.K. Wegahita, L. Ma, J. Liu, T. Huang, Q. Luo, J. Qian, Spatial assessment of groundwater quality and health risk of nitrogen pollution for shallow groundwater aquifer around Fuyang city, China, Water 12 (12) (2020) 3341.
[15] M.S. Khan, S. Kamal, M. Zulkiflain, M. Khalid, S. Khan, M. Shahid, M. Ahmad, Tailored coordination chemistry: a novel Zn (II)-fluorescent coordination material for highly selective and sensitive detection of Hg2+ ions in aqueous environments, J. Mol. Liq. 405 (2024) 125019.
[16] J. Dong, D. Zhao, Y. Lu, W.Y. Sun, Photoluminescent metal–organic frameworks and their application for sensing biomolecules, Journal of materials chemistry A 7 (40) (2019) 22744–22767.
[17] M.D. Allendorf, C.A. Bauer, R.K. Bhakta, R.J.T. Houk, Luminescent metal–organic frameworks, Chem. Soc. Rev. 38 (5) (2009) 1330–1352.
[18] X. Guo, G. Yue, J. Huang, C. Liu, Q. Zeng, L. Wang, Label-free simultaneous analysis of Fe (III) and ascorbic acid using fluorescence switching of ultrathin graphitic carbon nitride nanosheets, ACS applied materials & interfaces 10 (31) (2018) 26118–26127.
[19] L. Guo, Y. Liu, R. Kong, G. Chen, Z. Liu, F. Qu, L. Xia, W. Tan, A metal–organic framework as selectivity regulator for Fe3+ and ascorbic acid detection, Analytical chemistry 91 (19) (2019) 12453–12460.
[20] T. Wu, N. Prasetya, K. Li, Recent advances in aluminium-based metal-organic frameworks (MOF) and its membrane applications, J. Membr. Sci. 615 (2020) 118493.
[21] P. Su, L. Yu, Y. Ai, S. Zhang, H. Ge, Y. Bu, D. Huang, X. Wang, S. Wang, Conformational fixation induced fluorescence turn-on of oxytetracycline coordinated on aluminum-based metal-organic frameworks for ultrasensitive sensing application, Sensor. Actuator. B Chem. 368 (2022) 132043.
[22] L. Zhang, J. Wang, T. Du, W. Zhang, W. Zhu, C. Yang, T. Yue, J. Sun, T. Li, J. Wang, NH2-MIL-53 (Al) metal–organic framework as the smart platform for simultaneous high-performance detection and removal of Hg2+, Inorganic chemistry 58 (19) (2019) 12573–12581.
[23] C. Fan, X. Zhang, N. Li, C. Xu, R. Wu, B. Zhu, G. Zhang, S. Bi, Y. Fan, Zn-MOFs based luminescent sensors for selective and highly sensitive detection of Fe3+ and tetracycline antibiotic, J. Pharmaceut. Biomed. Anal. 188 (2020) 113444.
[24] M. Kaur, M. Yusuf, A.K. Malik, A luminescent Cu (II)-MOF with Lewis basic Schiff Base sites for the highly selective and sensitive detection of Fe3+ ions and nitrobenzene, Journal of Fluorescence 33 (1) (2023) 339–357.
[25] S. Fajal, P. Samanta, S. Dutta, S.K. Ghosh, Selective and sensitive recognition of Fe3 + ion by a Lewis basic functionalized chemically stable metal-organic framework (MOF), Inorg. Chim. Acta. 502 (2020) 119359.
[26] M.N. Lakhan, A. Hanan, Y. Wang, S. Liu, H. Arandiyan, Recent progress on nickel- and iron-based metallic organic frameworks for oxygen evolution reaction: a review, Langmuir 40 (5) (2024) 2465–2486.
[27] M.S. Khan, Y. Li, D.S. Li, J. Qiu, X. Xu, H.Y. Yang, A review of metal-organic framework (MOF) materials as an effective photocatalyst for degradation of organic pollutants, Nanoscale Adv. (2023).
[28] L.P. Hao, A. Hanan, R. Walvekar, M. Khalid, F. Bibi, W.Y. Wong, C. Prakash, Synergistic integration of MXene and metal-organic frameworks for enhanced electrocatalytic hydrogen evolution in an alkaline environment, Catalysts 13 (5) (2023) 802.
[29] A.E. Hoffman, L. Vanduyfhuys, I. Nevjestić, J. Wieme, S.M. Rogge, H. Depauw, P. Van Der Voort, H. Vrielinck, V. Van Speybroeck, Elucidating the vibrational fingerprint of the flexible metal–organic framework MIL-53 (Al) using a combined experimental/computational approach, J. Phys. Chem. C 122 (5) (2018) 2734–2746.
[30] I. Nevjestić, H. Depauw, P. Gast, P. Tack, D. Deduytsche, K. Leus, M. Van Landeghem, E. Goovaerts, L. Vincze, C. Detavernier, P. Van Der Voort, Sensing the framework state and guest molecules in MIL-53 (Al) via the electron paramagnetic resonance spectrum of V IV dopant ions, Phys. Chem. Chem. Phys. 19 (36) (2017) 24545–24554.
[31] C.X. Yang, H.B. Ren, X.P. Yan, Fluorescent metal–organic framework MIL-53 (Al) for highly selective and sensitive detection of Fe3+ in aqueous solution, Analytical chemistry 85 (15) (2013) 7441–7446.
[32] E. Rahmani, M. Rahmani, Al-based MIL-53 metal organic framework (MOF) as the new catalyst for Friedel–Crafts alkylation of benzene, Ind. Eng. Chem. Res. 57 (1) (2018) 169–178.
[33] P. Mishra, H.P. Uppara, B. Mandal, S. Gumma, Adsorption and separation of carbon dioxide using MIL-53 (Al) metal-organic framework, Ind. Eng. Chem. Res. 53 (51) (2014) 19747–19753.
[34] Y. Cui, Y. Yue, G. Qian, B. Chen, Luminescent functional metal–organic frameworks, Chemical reviews 112 (2) (2012) 1126–1162.
[35] Y. Zhou, H.H. Chen, B. Yan, An Eu 3+ post-functionalized nanosized metal–organic framework for cation exchange-based Fe3+-sensing in an aqueous environment, J. Mater. Chem. A 2 (33) (2014) 13691–13697.
[36] S.M. Kanan, A. Malkawi, Recent advances in nanocomposite luminescent metal-organic framework sensors for detecting metal ions, Comments Mod. Chem. 41 (1) (2021) 1–66.
[37] C.X. Yang, H.B. Ren, X.P. Yan, Fluorescent metal–organic framework MIL-53 (Al) for highly selective and sensitive detection of Fe3+ in aqueous solution, Analytical chemistry 85 (15) (2013) 7441–7446.
[38] Z.A. Zong, C.B. Fan, C.F. Bi, X. Zhang, R. Luo, X.M. Meng, F. Jin, Y.H. Fan, Highly selective functional luminescent sensor toward Cr (VI)/Fe (III) ion and nitrobenzene based on metal–organic frameworks: synthesis, structures, and properties, J. Solid State Chem. 270 (2019) 651–665.
[39] J.J. Perry IV, C.A. Bauer, M.D. Allendorf, Luminescent metal–organic frameworks. Metal-Organic Frameworks: Applications from Catalysis to Gas Storage, 2011, pp. 267–308.
[40] K. Kniec, W. Piotrowski, K. Ledwa, M. Suta, L.D. Carlos, L. Marciniak, From quencher to potent activator–Multimodal luminescence thermometry with Fe 3+ in the oxides MAl 4 O 7 (M= Ca, Sr, Ba), J. Mater. Chem. C 9 (19) (2021) 6268–6276.